# EMC Issues in High-Power Grid-Connected Photovoltaic Plants: An Update After 15 Years

Erika Stracqualursi, *Member, IEEE*, Gianfranco Di Lorenzo, *Member, IEEE*, Luigi Calcara, *Member, IEEE*, and Rodolfo Araneo, *Senior Member, IEEE*

***Abstract*—This article revises and updates the electromagnetic compatibility (EMC) challenges commonly encountered in utility-scale grid-connected photovoltaic (PV) systems in light of modern trends. This article examines the issues related to the conductive and radiated radio-frequency disturbances, in the range from 150 kHz to 1 GHz, of multi-MWp PV plants as designed nowadays, with high-power bifacial modules, single-axis trackers, and decentralized high-density inverters. The main features include the extensive dc and ac cabling, the capacitance toward the Earth of the PV source, the common-mode disturbance caused by inverters, the effect of safety and functional grounding, the galvanic isolation provided by step-up power transformers, and the presence of resonant circuits for common-mode leakage currents. Measurements in situ for both conducted and radiated disturbances in a 19.87 MWp plant placed in Ferrandina, South Italy, are presented and discussed. Guidelines for achieving an *EMC functional safety by design* are provided, raising from the analysis of the measured data.**

***Index Terms*—Conducted disturbances, electromagnetic compliance, photovoltaics, power conversion equipment, radiated disturbances, radio frequency noise, utility-scale plants.**

## I. Introduction

THE beginning of modern photovoltaic (PV) solar power dates back to the early 2000s when initial government incentives and feed-in tariff schemes [1] encouraged first grid-connected installations, paving the way to the dominance in the subsequent years of (multi)megawatt ground mount installations operated by utilities and stakeholders. In those pioneering years, system operators encountered multiple unexpected problems and failures during operation and maintenance [2], [3], resulting in unwanted risks and additional unbudgeted costs. These issues were caused not only by poor construction workmanship but also by deficient plant design due to the lack of expertise about the properties and operation of PV plants.

Manuscript received 11 January 2024; revised 4 June 2024; accepted 21 July 2024. Date of publication 5 September 2024; date of current version 28 October 2024. The work of Erika Stracqualursi was supported in part by the National Recovery and Resilience Plan (NRRP), Mission 4 Component 2 Investment 1.3 - Call for tender No. 1561 of 11.10.2022 of Ministero dell'Università e della Ricerca (MUR), by the European Union – NextGenerationEU (Project code PE0000021, Concession Decree No. 1561 of 11.10.2022 adopted by Ministero dell'Università e della Ricerca (MUR), CUP B53C22004070006, Project title "Network 4 Energy Sustainable Transition—NEST"). *(Corresponding author: Rodolfo Araneo.)*

The authors are with the Electrical Engineering Division of DIAEE, University of Rome, 00184 Rome, Italy (e-mail: rodolfo.araneo@uniroma1.it).

Color versions of one or more figures in this article are available at https://doi.org/10.1109/TEMC.2024.3440848.

Digital Object Identifier 10.1109/TEMC.2024.3440848

Among others, operators' concerns about electromagnetic compatibility (EMC) issues arose, especially regarding conducted disturbances. In [4], conducting research on a low-power 2.9 kWp PV plant, the authors addressed how the dc cables can act as a source of electromagnetic (EM) emissions generated by the commutation of power conversion equipment (PCE). In a PV plant, the deployment of electric/electronic equipment by different constructors gives rise to a complex system, where disturbances may affect the plant operation and performance or reach to public network [5], concerning nearby devices [6]. In those initial years, the primary source of disturbances was the PCE, i.e., the centralized solar inverter. However, the plant layout moved toward more sophisticated schemes with decentralized inverters up to string inverters in the following years. In addition, many other active devices were added to the PV plant for different purposes, such as to maximize the power production (PV string optimizers), restore panels affected by Partial Induced Degradation [7] (APID systems), and store energy [8] (battery storage systems).

In 2009, Araneo et al. [9] cast light on the effects of conducted disturbances in the range of 150 kHz–30 MHz in high-power PV plants, proposing guidelines and layout optimization to reduce the problem. In particular, the authors investigated in a 1 MWp power-rated PV plant the dominant EM phenomena and coupling mechanisms at the base of the generation of common-mode (CM) disturbances. The authors assessed the role played by some peculiar features of utility-scale PV plants, such as the extent of the dc cabling, the capacitance toward the Earth of the PV source, the noise generated by inverters, the galvanic isolation ensured by dedicated low-voltage (LV) power transformers, and the presence of resonant circuits for CM leakage currents.

In the infancy of PV solar power, the engineers were not properly supported by standards and guidelines that needed to be mature. Recommended best practices for a reliable layout from an EMC point of view were still missing. Only in recent years, standardization of EMC requirements for PV components has become more active. For instance, since 2008, the committee CISPR/B has examined the boundaries and measurement techniques for disturbances at dc ports of grid-connected power converters. The proposed limitations and measurement techniques were the foundation for the guidelines to enhance Std. CISPR 11, explicitly addressing the EMC requirements for PV power energy systems. The EMC specifications for PCE were included in the sixth edition of Std. CISPR 11 [10], released in 2015. Besides, certain product committees, which evaluate

items incorporating PCE, established their product standards regarding EMC requirements. IEC Std. 61800-3 [11] provides the boundaries and examination procedures of power drive systems (PDS). IEC Std. 62040-2 [12] regulates uninterrupted power supply, while Std. IEC 60974-10 [13] regulates arc welding. IEC Std. 62236 establishes the emission limitations for equipment operating within railway systems. IEC Stds. 61851-21-1 [14] and IEC Std. 61851-21-2 [15] address EMC criteria for ON/OFF-board equipment operating within conductive charging stations designed for electric vehicles.

Over the years, the power rate of PV systems has been increasing due to improvements in PV technologies, which mainly include a substantial increase in the power density of inverters (modern inverters began to use gallium nitride and silicon carbide (SiC) technology, which enables higher level of power density and efficiency compared to traditional silicon technology), an increase in the efficiency of PV panels, and the advent of efficient single-axis trackers. The passing of the grid parity [16] (achieved in the first 2010s by several European Countries) boosted the transition to high-power plants. Many policymakers removed subsidies and encouraged a self-sustaining market where investors look more favorably to utility-scale plants to take advantage of economies of scale. Meanwhile, the reduction of suitable land for ground-mounted PV plants, mainly due to the competition with crop production, pushed the construction of PV plants near sensitive installations, e.g., military installations and airports. As a result, there was an increasing concern that conducted and mainly radiated EM emissions could occur and affect the correct operation of crucial devices.

Notwithstanding the relevance of the ever-present subject, few papers have dealt with electromagnetic interference (EMI) in PV plants since [9]. Andersson et al. [17] conducted measurements of radiated emissions in a 3 kW PV installation in the range 3–500 MHz; the purpose is to assess the effect of solar power optimizers in combination with the PCE in terms of radiated EMI. Kubík and Skála [18] focused on the radiated EMI in the range 0.1–10 MHz of dc–dc converters for home applications. Interestingly, the radiated spectrum of inverters in the range of 0.1–1 MHz was used in [19] for power quality purposes to eliminate the need for existing monitoring infrastructure. Smolenski et al. [20] presented theoretical considerations about conducted EMI in multiconverter PV installations. They also present measurements conducted in the laboratory and on a 1 MWp plant. Conducted and radiated EMI, measured up to 1 GHz in a small roof-top PV installation, is also investigated in [21].

In this article, results are presented from a measurement campaign of conducted and radiated EMI in a modern 19.87 MWp PV plant with decentralized multilevel and transformerless PCE, bifacial monocrystalline half-cut N-Type Tunnel Oxide Passivated Contact (TOPCon) solar panels, and utility-grade single-axis trackers (see Fig. 1). This article revises and updates the EMC challenges commonly encountered in utility-scale grid-connected PV systems in light of modern design trends.

The rest of this article is organized as follows. In Section II, new design trends in utility-scale PV plants are revised. Section III addresses the fundamental EMI effects and mechanisms and the limits prescribed by main standards; the measurement campaign in the real PV system is described and the main results are discussed in Section IV. A discussion on design trends and guidelines regarding EMC issues is provided in Section V. Finally, Section VI concludes this article.

Fig. 1. Aerial view of the Ferrandina plant.

## II. New Trends in Utility-Scale PV Plants

### A. New Manufacturer Trends for PV Technologies

Since the publication of [9], the design and construction of utility-scale PV plants have changed remarkably due to improvements in technologies that opened new ways of thinking about PV solar plants. These changes, which will be recalled in reference to the Ferrandina PV plant, also impact the EMI, which can occur in a modern PV plant.

Nowadays, bifacial solar panels have become a standard choice [22]. Both front and rear surfaces are covered with PV cells and used for power generation. The bifacility yields a power generation gain that mainly increases with the increase of the diffuse component of the solar irradiance (thus with latitude), the albedo of the site, the installation height of the modules, and the row distance (lower ground coverage factor). Since improvements in the plant's performance ratio usually come along with the growth of the overall costs, the design phase always requires a trade-off assessment between the performance ratio and the capital and operational expenditures, which are all included in the levelized cost of electricity.

As concerns module technology, today PV modules are based on N-type TOPCon cells [23]. The base layer is N-type, doped with phosphorus. The generated free electrons are responsible for extremely low power losses, thus leading to higher efficiencies, and they prevent phenomena, such as partial and light induced degradation. TOPCon technology is considered the next generation of the Passivated Emitter Rear Contact (PERC) technology [24] of which it can be viewed as an upgraded version. Manufacturers of PERC cells that wish to enhance their current manufacturing lines will require less capital investment with respect to other available technologies, e.g., hetero-junction or interdigitated back contact solar cells. Finally, the modern modules are all based on the half-cut cells technology, which reduces losses, stress, and possible cracking and improves shading tolerance and lifespans. One of the most diffused module series employs 144 half-cut cells and reaches a rated power at Standard Test Conditions around 580–590 Wp with dimensions 2278 $\times$ 1134 mm. The Ferrandina plant comprises 1377 strings of 26 modules connected in series, type Suntech Ultra V STP 555 S-C72/Nmh+ [see Fig. 2(a)].

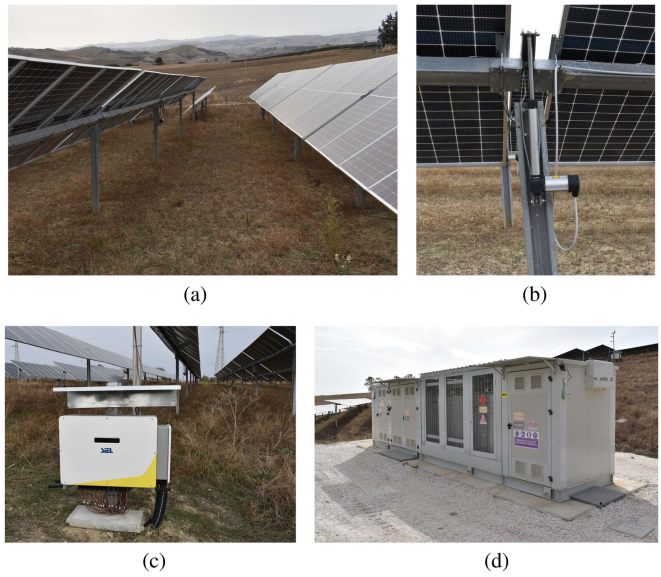

Fig. 2. New manufacturer trends in utility-scale PV plants. (a) Suntech STP 555 S-C72/Nmh+. (b) Convert TRJ actuator. (c) SIEL Soleil SPX 250 K-3ph. (d) MV Skid.

The bifacial modules perform best with dual- or single-axis trackers [25] and decentralized inverters with multiple maximum power point trackers (MPPTs).

Despite achieving the highest energy generation, dual-axis trackers still need to be more affordable, making them less cost-effective [26]. Moreover, they proved to suffer from the wind load pressure, affecting trackers' stability and reliability, which increased with the use of large-format modules. On the contrary, the single-axis trackers proved to be a robust and cost-effective solution [27]. Being available in one-in-portrait (1P) and two-in-portrait (2P) formats, the manufacturer's trend is preferring to use 1P trackers with large module panels, e.g., 144 or 156 half-cut cells. That is mainly because the increased wind force generated by larger modules does not compromise their traditional benefits, such as their ramming ability and smaller tracker height. Usually, the drive system comprises a linear actuator per row, driven by an ac (brushless) motor [28]. The Ferrandina plant employs 2P Convert TRJ single-axis trackers that accept 52, 26, and 13 modules [see Fig. 2(a) and (b)].

Decentralized inverters with multiple MPPTs are becoming the new standard in utility-scale plants, mainly when used in conjunction with trackers. Decentralized inverters are close to the string inverters, where a single inverter with its own MPPT is connected to a single string. Defined as multiple string inverters in [29], they have multiple lower power dc–dc converters with their independent input EMI filter and MPPT. Each converter has a low number of PV inputs, usually from one to four. All dc–dc converters are connected via a dc bus to a single multilevel dc–ac inverter controlled via pulsewidth modulation (PWM) with a single EMI filter at the output. The modern inverters reach a power density of 3 kW/kg and are commercially available with rated powers up to 330 kW and dimensions around $1050 \times 750 \times 400$ mm. The decentralized inverters usually work within 1500 Vdc. They are connected at LV 800 Vac through three-phase connections (without neutral conductor) to centralized compact medium voltage (MV) skids. Each skid includes an LV/MV oil-immersed transformer, MV gas-insulated switchgear, all necessary LV protections to connect the PV arrays, and available auxiliary services with independent auxiliary power at 400 Vac. The MV output level of the skids depends on the type of grid connection to reduce the number of transformers needed. In Italy, 20 kV is used for connection to the MV distribution grid, 36 kV is used for high voltage (HV) low power connections (below 125 MVA–100 MW), and 30 kV is used for connections to the HV network at 150 kV through MV/HV transformers and air-insulated, GIS insulated or compact hybrid switchgear (see the report titled "The hypergrid project and development requirements" written by the Italian Trasmission System operator Terna S.p.A. [30]). The Ferrandina plant comprises 78 decentralized inverters, SIEL Soleil SPX 250 K-3ph rated power 250 kW in ac, with 24 string inputs and 12 MPPTs; they are connected to three MV skids with 30 kV output voltage [see Fig. 2(c) and (d)]. The grid connection is at 150 kV with an independent interconnection substation placed 14 km away from the PV field.

### B. New Design Aspects

The way of designing a PV system has changed remarkably since the early years at the beginning of the 2000s. With reference to Fig. 3, today, the strings are designed long enough to work at a maximum open-circuit voltage (at the minimum temperature of the site) of 1500 Vdc to reduce the currents in the PV generator and, consequently, ohmic losses. The combiner boxes used to parallel PV strings are not used anymore in a decentralized solution since the strings are directly connected to the dc inputs of the decentralized inverters. The three-phase three-wires ac outputs of the decentralized inverters, usually operated at 800 Vac, can run through the PV generator for more than 100 m up to the inputs of the LV/MV skid. According to European practice (see IEC Std. 60364-1), the dc field is operated isolated from Earth.

Regarding the ac power system, the grounding practice is much less well-defined: the power system can be designed to be operated solidly grounded or ungrounded. In the former case, one can take advantage of the improved protection provided by built-in ground-fault trip mechanisms available in most LV power circuit breakers to detect faults easily. In the latter case, the advantage lies in maintaining service on the entire system under the first fault, yet an insulation monitoring device is required [31].

The output of the decentralized inverters are parallel connected on an LV panelboard placed in the skid, acting as an LV collector. In the same skid, a power transformer steps the voltage up from 800 Vac to MV/HV ranging from 20 to 36 kV, depending on the type of grid connection. From the LV panelboard, a step-down transformer is employed to feed the auxiliary services operated at 400 Vac, which can be fed also by an emergency auxiliary generator. The service panelboard supplies mainly power to the trackers' drives. An uninterruptible power supply and a

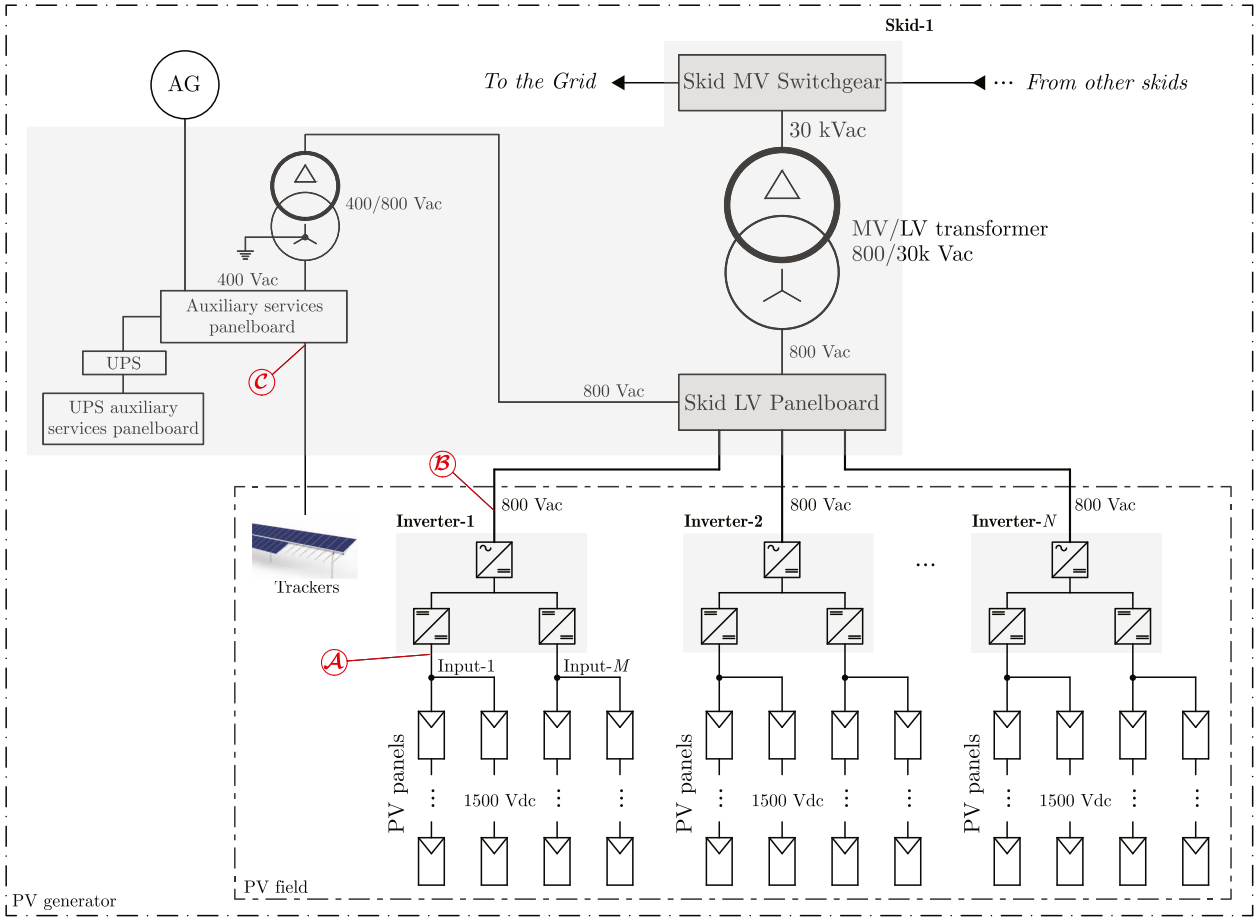


Fig. 3. Simplified single line diagram of the PV system of Ferrandina.

continuity service panelboard are needed to supply power to the fundamental monitoring, control, and security systems. The MV/HV ac collection system is then connected to the electric utility at a point-of-interconnection; larger plants may have an independent interconnection substation.

## III. EMI Characterization

### A. Radio-Frequency (RF) Characterization

Due to the new trends and design practices discussed in the previous sections, the RF characterization of a modern utility-scale PV system has been changed with respect to what is explained in [9], in some salient aspects that need to be evaluated and monitored. More recently, the radiation effects have emerged as a major concern and cannot be disregarded anymore because several new plants have been constructed near military installations, airports, or communication facilities sensitive to EM disturbances. The issue of controlling radiated and CM conducted disturbances, and particularly how to deal with EMC issues, safety, and continuity of service simultaneously, is complicated by conflicting philosophies advocated by people of different backgrounds. Power-oriented and EMC-oriented engineers often differ in their perception of the problem and potential solutions.

Disturbances can propagate throughout the PV system along different stray paths depicted in Fig. 4.

The capacitance to the Earth of the PV modules dictates the behavior of the dc PV field, providing an intricate pattern for CM leakage currents (letter $\mathcal{A}$ in Fig. 4). As illustrated in [32] and [33], a rack-mounted PV module has six different capacitances. Since the aluminum frame and the rack are always grounded according to the recommended practices (see the recent IEEE Std. 2778-202 [34]), only three terms remain, namely the cell-to-frame capacitance $C_{\mathrm{cf}}$, the cell-to-rack capacitance $C_{\mathrm{cr}}$, and the cell-to-ground capacitance $C_{\mathrm{cg}}$. The whole zero-sequence capacitance may reach values of several $\mathrm{pF/m^2}$; under the rain, when water can cover the module surface and is in contact with the aluminum frame, the parasitic capacitance can increase by 30 times. Using frameless modules, e.g., some thin-film modules, alleviates the problem. To the best of the authors' knowledge, the bifacial modules do not present any relevant change in the zero-sequence capacitance of the plant.

The long wiring on the ac side of the inverters (usually at 800 Vac) that occurs due to their decentralization throughout the field, provides a new path for disturbances coupling and radiation (letter $\mathcal{D}$ in Fig. 4). It adds in parallel to the wiring on the dc side of the inverters (letter $\mathcal{B}$ in Fig. 4). The length of both the lines may reach 150–200 m, lowering the frequencies of

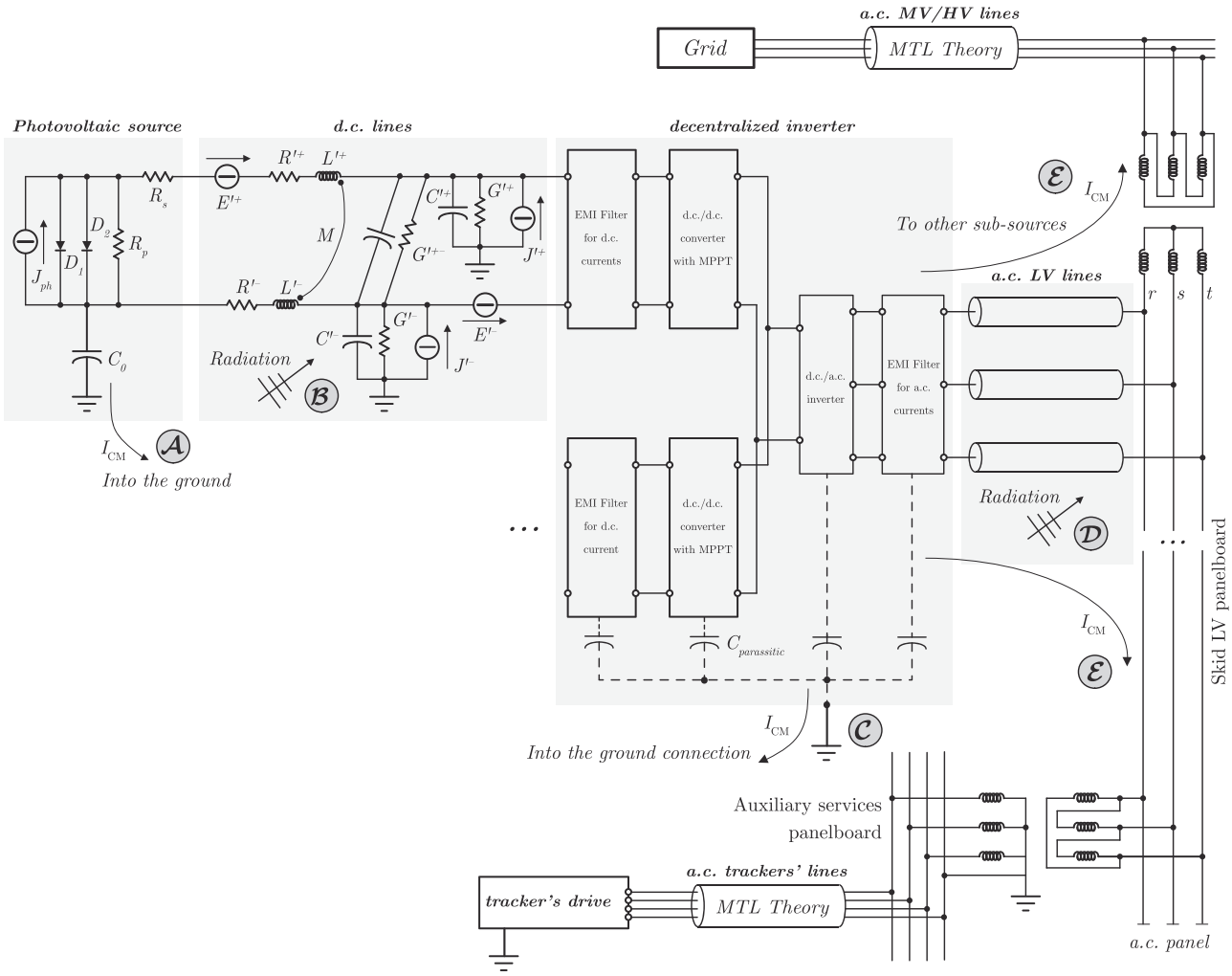


Fig. 4. Equivalent circuit of a PV source.

possible resonant effects near quarter-wavelength and radiation effects near half-wavelength below 1 MHz.

The noise voltage on wirings is influenced by the functional grounding of the dc and ac systems [31]. Attention must be drawn to the fact that modern (decentralized) inverters do not provide galvanic isolation between the dc and ac sides. According to IEC Std. 60364, the functional grounding of a dc live conductor of the PV array is allowed only if the galvanic separation between dc and ac sides of the PV system is present (i.e., there is a separation transformer). Usually, the dc array is operated ungrounded, except in a few cases, mainly in the USA, where some manufacturers of PV modules require positive or negative grounding of the PV generator when using thin-film and back-contact PV modules; instead, on the ac side, three-phase, three-wire solidly grounded or ungrounded wye system are employed. Generally speaking, solidly grounded systems ensure a stable zero-voltage reference point, which reduces CM voltage noise but, reversely, provides an effective conductive path to Earth for electrical noise currents, which could be a source of radiated EM emissions.

Decentralized inverters produce CM noise in the same manner as centralized inverters. Accurate CM noise models are necessary for studying effective solutions to comply with the maximum EM noise levels that the standards allow [35]. In modern inverters, SiC devices have pushed switching frequency well above 150 kHz, increasing the magnitude of the CM disturbances in the 150 kHz–30 MHz range due to higher time derivatives of voltage, $\mathrm{d}v/\mathrm{d}t$, and current, $\mathrm{d}i/\mathrm{d}t$. Since passive filters are experiencing difficulties in reducing noise above 1 MHz, much research focuses on active noise reduction techniques [36]. According to the authors' experience, attention must be paid to the ground connection of the wye ac system at 800 Vac when present (i.e., ac system operated solidly grounded) because a skid LV panelboard (see Fig. 3) can easily collect around $20 \div 30$ decentralized inverters. The noise currents on the bonding system jumper can exceed the limits required by the standard.

Finally, stray CM currents could flow to other equipment through the entire PV plant (letter $\mathcal{E}$ in Fig. 4). Anyway, step-up power transformers, which have an intrinsic low-pass behavior, alleviate the problem. Attention must be drawn to CM noise

TABLE I
LIMITS FOR CONDUCTED DISTURBANCES OF CLASS A GROUP 1 EQUIPMENT MEASURED ON A TEST SITE ACCORDING TO STD. CISPR 11 AND IEC STD. 61800-3

| Frequency range | Voltage limits Rated power > 75 kVA | | | |
|---|---|---|---|---|
| | ac | | dc | |
| | QP | AV | QP | AV |
| MHz | dB ($\mu$V) | dB ($\mu$V) | dB ($\mu$V) | dB ($\mu$V) |
| 0.15–0.50 | 130 | 120 | 132@0.15 MHz | 122@0.15 MHz |
| 0.50–5 | 125 | 115 | 122@5 MHz | 112@0.15 MHz |
| 5–30 | 115 | 105 | 122–105 | 112–92 |

TABLE II
EM RADIATION DISTURBANCES LIMITS FOR EQUIPMENT MEASURED ON A TEST SITE

| Frequency range | Electric field limits | | | |
|---|---|---|---|---|
| | Std. CISPR 11 Class A Group 1 rated power > 20 kVA | | IEC Std. 61800-3 PDS of category C3 in the second environment | |
| | Measuring distance | | Measuring distance | |
| | 10 m | 3 m | 10 m | 3 m |
| MHz | QP dB ($\frac{\mu V}{m}$) | AV dB ($\frac{\mu V}{m}$) | QP dB ($\frac{\mu V}{m}$) | AV dB ($\frac{\mu V}{m}$) |
| 30–230 | 50 | 60 | 50 | 60 |
| 230–1000 | 50 | 60 | 60 | 70 |

TABLE III
EM RADIATION DISTURBANCES LIMITS FOR CLASS A GROUP 1 EQUIPMENT MEASURED IN SITU ACCORDING TO STD. CISPR 11 AND IEC STD. 61800-3

| Frequency range | Disturbances limits Measuring distance 30 m | |
|---|---|---|
| | Electric field QP | Magnetic field QP |
| MHz | dB ($\mu$V/m) | dB ($\mu$A/m) |
| 0.15–0.49 | – | 13.5 |
| 0.49–3.95 | – | 3.5 |
| 3.95–20 | – | –11.5 |
| 20–30 | – | –21.5 |
| 30–230 | 30 | – |
| 230–1000 | 37 | – |

induced through ground loops formed by the metal MV/HV cable armors/shields. The bonding arrangement of the sheaths of these cables, according to IEEE Std. 575 [37], i.e., solid bounding, single-point bonding, or cross-bonding, must be carefully evaluated. No attempt will be made here to delve into such matters in detail, except to convey the depth of the problem that transferred disturbances can entail in the presence of an HV substation external to the PV field, even tens of kilometers away.

### B. Standard Limits

The Std. CISPR 11 [10] (see also Std. EN 55011) remains the milestone for EM disturbances by industrial, scientific, and medical equipment. The first edition was released in 1975, and the standards reached the sixth edition in 2015. The edition continues the long-standing practice of Group 1–Group 2 and Class A–Class B equipment classifications. In utility-scale PV plants, designers must fulfill the requirements for Class A—Group 1 equipment.

1) Class A equipment is appropriate for use in all settings except for residential environments and areas directly connected to an LV power supply network that serves buildings used for domestic purposes.
2) Group 1 equipment contains all equipment in the scope of the standard, which is not classified as Group 2 equipment. Semiconductor rectifiers/inverters and grid-connected power converters are explicitly listed among Group 1 equipment.

The quasi-peak (QP) and average (AV) limits prescribed by the Std. CISPR 11 for the voltage magnitude of conducted disturbances in the range 150 kHz–30 MHz (for equipment with rated power greater than 75 kVA) and for the electric field magnitude of radiated disturbances in the range 30–1000 MHz (for equipment with rated power greater than 20 kVA) are reported in Tables I and II, respectively.

The limits are almost the same as those prescribed by the IEC Std. 61800-3 [11] for PDS of category C3 with $I > 100$ A.[1] The limits prescribed by Std. CISPR 11 have been referred to also in the IEC Std. 62920 [38], conceived explicitly for PCE in PV systems. They apply to PCE of Class A, suitable in nonresidential environments.

When performing in situ measurements, as reported in the following section, the limits for the electric and magnetic fields are reported in Table III at a distance of 30 m from the plant.

Particular attention must be drawn to the trackers' drives. Machine tools are listed in Group 1 equipment of Std. CISPR 11 so that they could fall under the prescription of Std. CISPR 11. Yet, some inspectors or operators may want to apply the prescription of IEC Std. 61000-6-4 [39], which is generally mandatory for equipment connected to the LV ac power system in an industrial environment. The limits are more severe than those of Std. CISPR 11, and they are not easily met.

## IV. ON-SITE MEASUREMENTS

### A. Conducted EMI

The measurements of the conducted disturbances have been performed, as already done in [9], according to the Std. CISPR 16, using an EMI Receiver PMM ER9000 and a voltage probe PMM SHC-1.

Initially, the conducted disturbances produced by the decentralized inverters were monitored on the dc and ac sides, performing several measurements on the inputs and outputs of some of the 68 inverters in sample surveys. Fig. 5 shows two representative results of the measurement campaign: the measurement results on a dc input in Fig. 5(a) (point $\mathcal{A}$ in Fig. 3) and on an ac output in Fig. 5(b) (point $\mathcal{B}$ in Fig. 3), with the limits prescribed by the standards. The disturbance level is well

[1] A PDS of category C3 is of rated voltage less than 1000 V and intended only for use in the second environment. The second environment includes all establishments other than those directly connected to an LV power supply network that supplies buildings used for residential purposes.

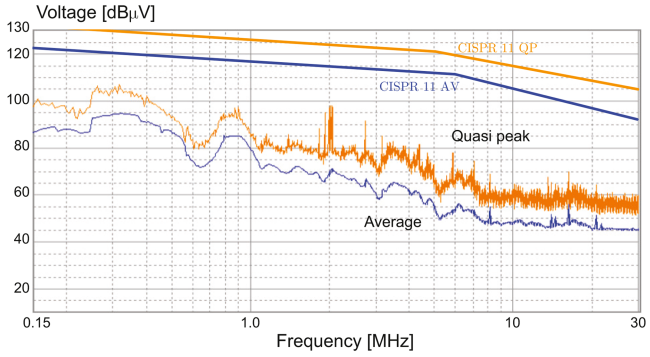


(a)

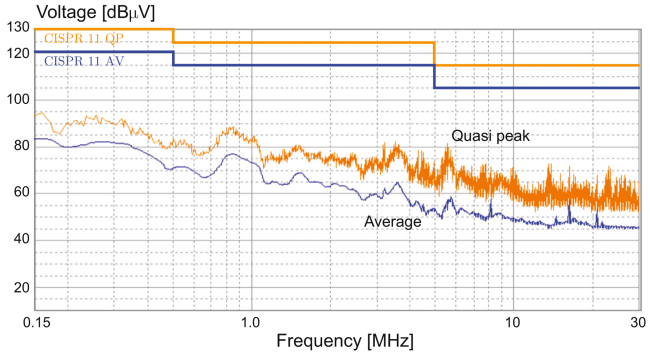


(b)

Fig. 5. CM disturbance voltage measured at (a) DC input and (b) AC output terminals of a decentralized inverter.

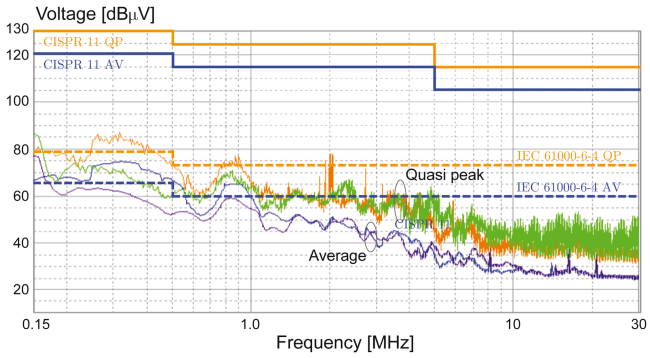


Fig. 6. CM disturbance voltage measured at the terminals of two circuit-breakers feeding two power lines of trackers' drive: orange-blue lines are for a 180 m long line; green-violet lines are for a 65 m long line.

below the limits; no critical aspect is observed. Remarkably, the noise level is quite the same on dc and ac sides in terms of voltage.

Then, the disturbance measured on the feeding points of the trackers' drive power lines, at the terminals of the circuit breakers installed on the skid LV panelboard for auxiliary services (point $\mathcal{C}$ in Fig. 3), was characterized. Fig. 6 shows a representative result for two circuit-breakers whose lines are of different lengths. As previously explained, the applicable standard limits can be different: compliance is obtained only with the requirements of CISPR 11; if the requirements of IEC Std. 61000-6-4 are

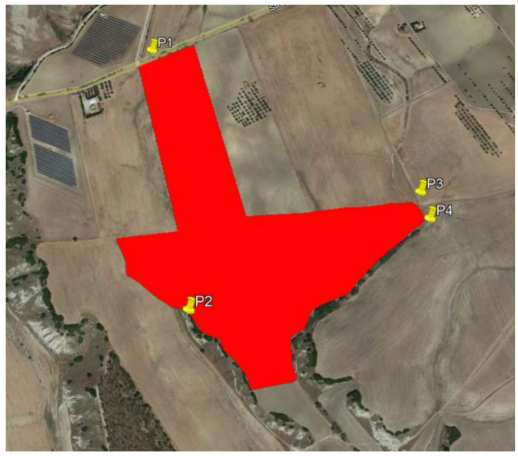


(a)

(b)

Fig. 7. (a) Measurement locations for radiated EMI; (b) Field layout.

considered, installation of filters effective below 2 MHz would turn necessary, as explained in [9].

### B. Radiated EMI

The measurement campaign of radiated EM disturbances comprised the measurement of the magnetic and electric field in four points—namely, P1, P2, P3, and P4 as shown in Fig. 7(a)—as required by art. 10 of Std. CISPR 11, placed at a distance of 30 m from the external fence of the PV field considered as equipment under test (EUT). The layout of the PV field is reported in Fig. 7(b). The measurements were performed using the following certified equipment.

1) EMC analyzer PMM ER8000.
2) Active loop antenna Com-Power AL-130R in the range 150 kHz–30 MHz.
3) Biconical antenna PMM BC-01 in the range 30 MHz–200 MHz.
4) Log periodic antenna PMM LP-02 in the range 200 MHz–1 GHz.

Measurements were performed for the magnetic field's $x, y$, and $z$-components in the low-frequency range and for both

Fig. 8. Pictures of the in situ measurements.

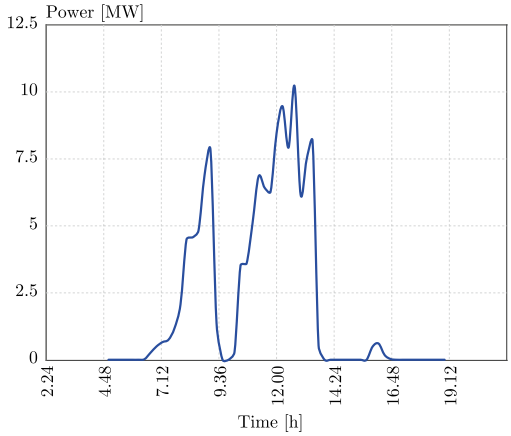


Fig. 9. Power produced by the field measured at the HV 30 kV interconnect point during the day of the test measurements.

vertical and horizontal polarization (VP and HP) of the electric field in the high-frequency range. Both the background noise with the EUT switched-OFF and the radiated disturbances with the EUT switched-ON were measured. The results were obtained by performing ten subsequent measurements to better identify the emissions due to the EUT. During and after the test, the apparatus continued to operate as intended; no performance degradation or loss of function was observed. The expanded uncertainty of the measurement results with coverage factor $k = 2$ and confidence level $p = 95\%$ is 4.35 dB in the range 0.15–30 MHz, 4.33 dB in the range 30–200 MHz, and 5.43 dB in the range 0.2–1 GHz.

As shown in Fig. 8, performing such measurements is not easy since the PV plants are placed in agricultural areas that are not easily accessible by the car, which contains the auxiliary generator for the instruments. Moreover, switching OFF these plants to measure the ambient noise is a matter of discussion with the property, since the revenue loss may reach 3000 €/hour.

The measurements were conducted on a sunny day in October 2023. Fig. 9 shows the time trend of the power produced by the PV plant during the day of the test measurements. The power is measured at the 30 kV ac interconnect point between the field and the HV line toward the HV grid substation. The power produced by the plant during the four measurements was 6.84 MW in P1 (time around 10:45 A.M.), 9.56 MW in P2 (time around 12:15 A.M.), 7.46 MW in P3 (time around 1:30 P.M.), and 0.49 MW in P4 (time around 4:30 P.M.).

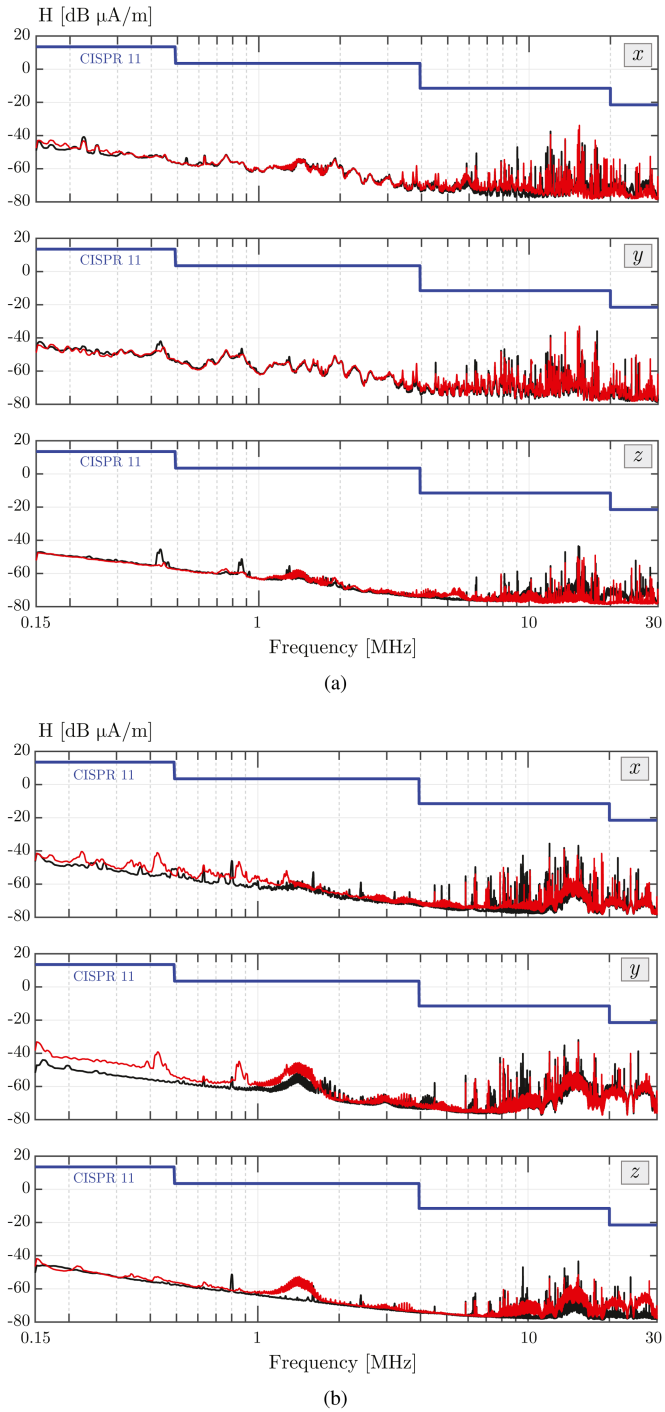


Fig. 10. Magnetic field background noise (red curve) and radiated disturbances (black curve) in the range 0.15–30 MHz at points: (a) P1, (b) P2.

Fig. 10 shows the value of the three components of the magnetic field measured in the range 0.15–30 MHz at points P1 and P2. Fig. 11 shows the value of the vertical and horizontal polarization of the electric field measured in the range 30–200 MHz at points P1, P2, and P3. Finally, Fig. 12 shows the value of the vertical and horizontal polarization of the electric

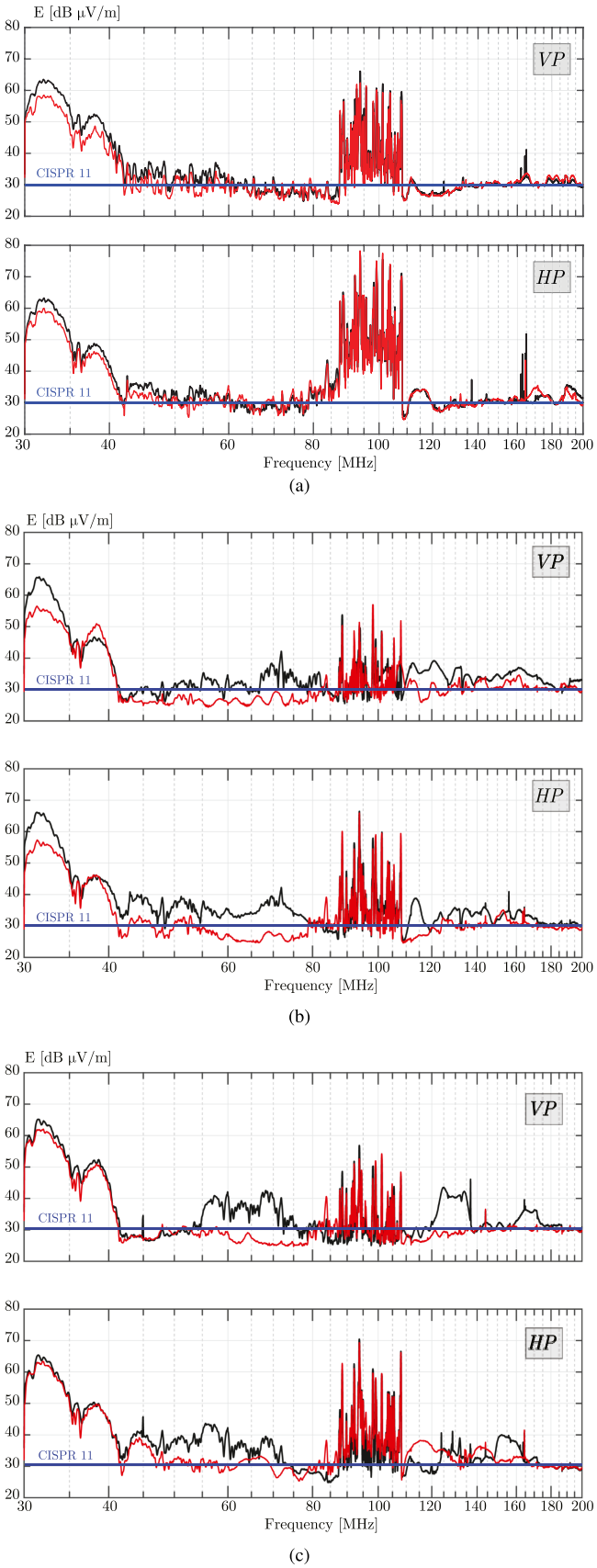


Fig. 11. Electric field background noise (red curve) and radiated disturbances (black curve) in the range 30–200 MHz at points: (a) P1, (b) P2, (c) P3.

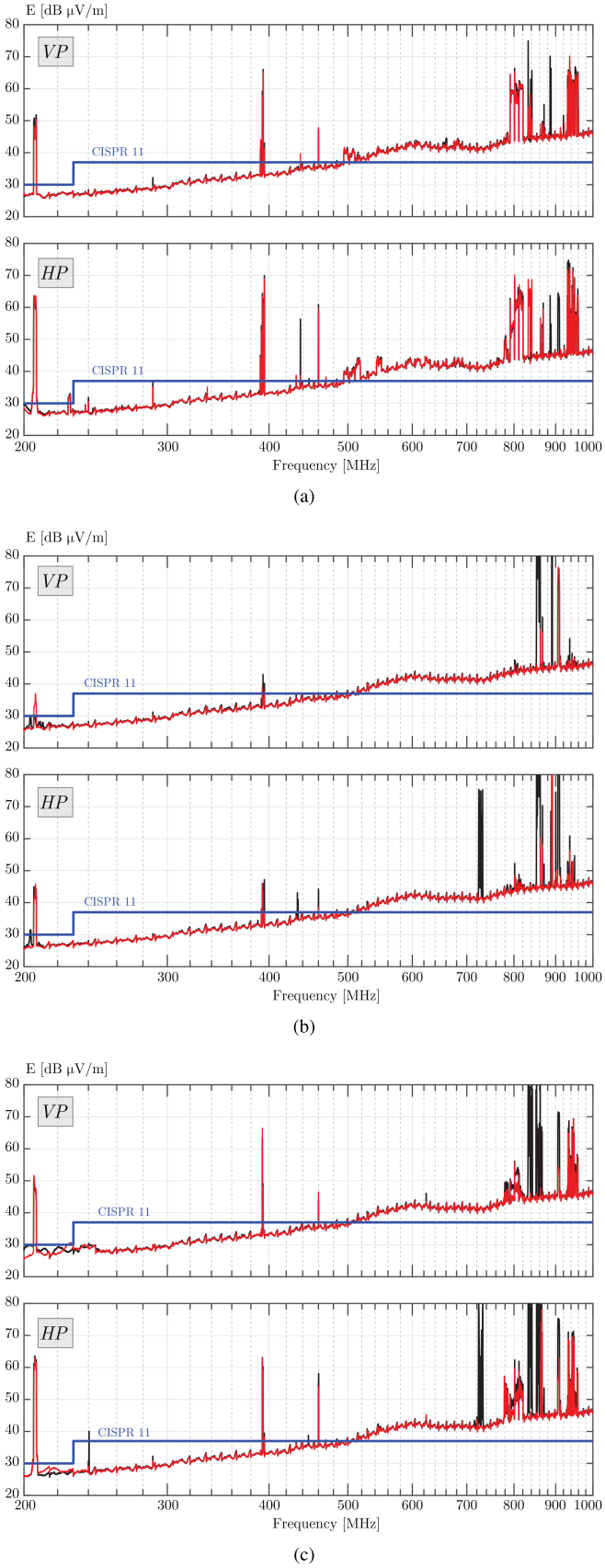


Fig. 12. Electric field background noise (red curve) and radiated disturbances (black curve) in the range 0.2–1 GHz at points: (a) P1, (b) P2, (c) P3.

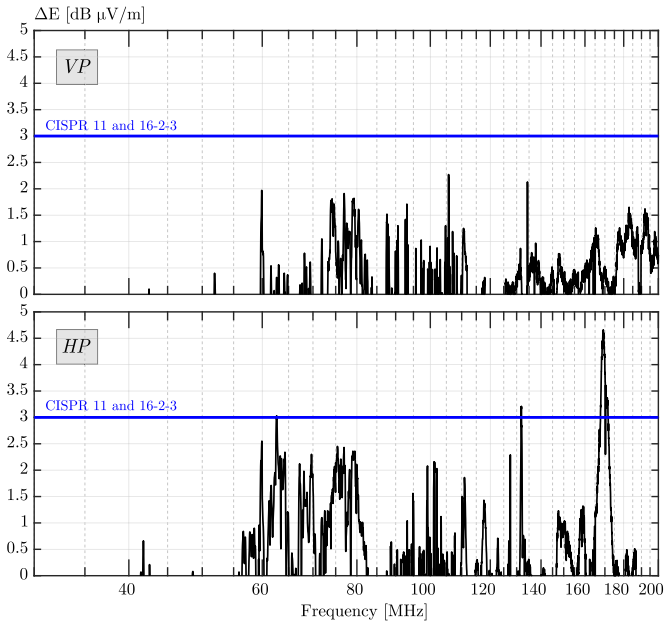


Fig. 13. Emission level with respect to the noise floor at point P1 in the range 30–200 MHz.

field measured in the range 200–1000 MHz at points P1, P2, and P3.

Some remarks are possible. The measurements in the range 0.15–30 MHz are not critical, since the radiated disturbances are always well below the limits allowed by the standards. The limit of background ambient noise is always at least 10 dB below the reference limits. The radiation is insensitive to the point of measurement and the power produced by the field. It was not identified any critical issue, since the radiated disturbances were always well below the limits allowed by the standards. An increase in the value of the radiated EM disturbance is observed above 1 MHz.

The measurements in situ above 30 MHz are always challenging since they are usually affected by high ambient noise. In fact, the range 87.5–108 MHz is affected by emissions from broadcasting FM transmitters, while the range 200–1000 MHz is affected by emissions from television signal broadcasters and radio base stations for mobile phones. As a rule of thumb, ambient noise should be at least 6 dB below the reference level. If the background noise level exceeds the reference level, the emissions of the EUT shall not increase this noise floor by more than 3 dB. Anyway, the computation of the increase requires the subtraction of the ambient noise level, measured with the EUT switched-OFF, from the disturbance level, measured with the EUT switched-ON, as done, for instance, for the electric field in the range 30–200 MHz at P1, and shown in Fig. 13. The point is that such a difference is unstable and not repeatable because it depends on the time needed to switch the power plant ON (or OFF). In a PV system like Ferrandina, consisting of about 68 inverters distributed over 24 hectares, around 15–20 min were needed to switch-OFF all the inverters. To reduce the time between the measurement of the radiated disturbances and the background noise, it is advisable to measure first the emission when the system is ON and then the ambient noise when it is OFF, as turning ON the inverters takes more time. Once connected, the inverters must synchronize the frequency and the output voltage to the grid before resuming power generation in ac.

TABLE IV
ELECTRIC FIELD MAGNITUDE IN THE FREQUENCY RANGE 100 KHZ–3 GHZ

| Point | Electric field magnitude V/m |
|---|---|
| Near dc cables of PV strings | 37 |
| Near trackers' drive | 8 |
| Near inputs of decentralized inverters | 80 |
| Near skid LV panelboard at 800 Vac | 55 |
| Near skid service LV panelboard at 400 Vac | 42 |
| Near MV cables running through the plant | 3 |

Annex A of the Std. CISPR 16-2-3 [40] provides some informative material about the measurement of disturbances in the presence of ambient noise when performing in situ tests in open-area sites. The standard differentiates the methods to be adopted depending on the type of ambient noise, which can be narrowband or broadband. The standard suggests performing some pretestings in a shielded room when possible. In addition, it suggests to repeat the measurements in the open site changing the detector (QP or AV) and choosing the bandwidth to minimize the measurement error. Yet, even doing this, the separation between disturbance and ambient noise is only sometimes possible. The subject is too broad to be treated here, and the interested reader is referred to the Annex. What the standard suggests is very difficult and time-consuming to perform on a utility-scale PV plant, where reducing the time the plant is switched-OFF is mandatory.

From the measurement results, an evident increase is observed in the emissions in the 40–80 MHz range at points P2 and P3 (see Fig. 11), which are close to the skids. Moreover, an increase in the disturbance is observed also around 900 MHz (see Fig. 12). All the inverters are connected via RS485-Modbus RTU to the skid and via WiFi to mobile receivers at the disposal of the maintenance personnel. The general packet radio service (GPRS) transmitters are placed on the skids and work at 850/900/1800/1900 MHz.

Finally, the electric field in the frequency range 100 kHz–3 GHz was scanned inside the PV system using an EM field sensor PMM EP330 and a field meter PMM 8053-B. The observed electric field intensities are reported in Table IV.

## V. DISCUSSION: LATEST DESIGN TRENDS, GUIDELINES, AND FUTURE PERSPECTIVES

The ongoing trend in utility-scale PV systems is moving toward large installations and high power densities to reduce the levelized cost of energy and reduce the break-even point over which a project becomes profitable. To this end, over the last 15 years, new components have been tested and today have become common parts of modern PV systems (e.g., single-axis trackers, decentralized inverters, power skids). Hence, PV systems have seen an increase in the number and variety of power components

deployed in the field, in the number of power distribution systems and voltage levels they require, and an increase in wiring, earthing, and bonding complexity [41].

At the same time, EMC emission and interference have emerged as serious problems, increasing significantly in intensity and frequency of occurrence. The proliferation of power devices that generate EM disturbances and electronic devices (mainly for monitoring purposes) that are susceptible to interfering signals makes it difficult to achieve EMC in modern PV systems.

In the last decades, the fundamental mechanisms leading to conducted disturbances, CM radiation, and, generally, EMI related to PV systems have not changed, and the comprehension of these mechanisms requires just a solid knowledge of the fundamentals of EMC theory and practice.

Anyway, utility-scale PV systems show some peculiarities that have become increasingly marked with the recent evolutions in the PV industry; they can be summarised as follows.

1) The coexistence of long dc and ac wiring of power and signal cables, intensified with respect to the past by the decentralization of the inverters and the feeding and control of the trackers.
2) The presence and proximity of cables operated at very different voltage levels, ranging from extra-LV levels (for monitoring and control) to HV levels (for power connection), due to the aforementioned reasons and also to the spread of the skids over the field.
3) The presence of a complex earthing and bonding system, due to the presence of many metal structures that call for an accurate classification as exposed-conductive-parts or extraneous-conductive-parts.
4) The proximity of high-power density devices for power conversion and susceptible electronic systems for monitoring and control.
5) The development of the electric system mainly in the open field.

All these features require serious attention in the correct cable routing, raise the need for an accurate earthing and bonding design, call for the protection from lightning threats, and pose severe problems in evaluating radiated and conducted disturbances to reach compliance with EMC standards.

Obtaining an *EMC functional safety by design* is a formidable task. Indeed, the ways of designing a PV system are so varied, and the power, monitoring, and security systems can be so different that caution must be exercised in providing general guidelines. Anyway, an attempt can be made.

An effective grounding system that provides a low-impedance bond to the equipment (e.g., modules, trackers, decentralized inverters, panelboards, etc.) throughout the field is paramount. It is necessary to find a trade-off between power system designers, acting according to safety criteria for personnel at the industrial frequency (e.g., by verifying step and touch voltages [42]), and EMC designers, addressing high-frequency noise, conducted and radiated disturbances, and equipment functionality. The new IEEE Std. 2778 is suggested as a valuable source of information and instructions. It is necessary to prevent conductive ground loops from being established by error or oversight through ground bounding and shields of power and signal cables. It is suggested to use a single Earth grounding electrode extending over the entire field and keeping the length of equipment grounding conductors as short as possible. At the neutral-to-ground bonding jumper (functional grounding) requested by wye transformers with solidly grounded neutral, the earthing electrode around the equipment pad should be improved with rings, meshes, and vertical rods to reduce the ground potential rise and avoid a noisy ground. A design that is not confined to the power frequency but also looks at the behavior of the grounding system at higher frequencies [43], [44] is encouraged; appropriate commercial (e.g., XGSLAB [45]) and custom software is available for this purpose (e.g., Grounding Electromagnetic Analysis Simulator [46]).

Metallic cable trays and raceways are not frequently used in modern PV plants due to limitations on the economic budget dictated by grid parity. Usually, the designers prefer to fix cables directly to the trackers' vertical poles or horizontal support posts or use nonmetallic buried conduits, directly buried cables when possible, or concrete cable troughs. Consequently, shielding effects (yet often poor) associated with the use of galvanized steel (effective at low frequency) or aluminum (effective at higher frequencies) are not exploitable. The design of an accurate routing that prevents loops is the only feasible way to reduce radiated EMI and susceptibility. For communication systems (e.g., required by inverters), it is preferable to use shielded cables with the shield grounded at both ends or, better, to use optic fibers that can be routed with power cables. Attention should be paid to the strength level of WiFi communication channels provided by modern inverters and GPRS channels used for the remote control of the field.

The accurate location of distributed inverters should be evaluated in presence of susceptible installations located close to the PV field. Usually, they are placed barycentric to the array formed by the PV strings that are connected to them. A nonbarycentric placement is a possible choice to keep a sufficient distance from the installation sensitive to EMI.

Passive shielding [47] can be used in the presence of nearby sensitive installations that require the highest protection level. Passive shielding is suitable for shielding skids, technical rooms containing power converters, or encasing decentralized inverters in small shielded boxes, taking care of thermal effects. Shielding materials effective in the RF range are available on the market (the shielding effectiveness is more than 100 db). For instance, a copper/aluminum sandwich material provided by G-Iron (under the name MRI) has been employed with optimal results (see Fig. 14). It also provides very easy and quick installation since the material is rolled and cut according to the needs.

Passive shielding can also be used per power and signal cables using classical underground shielded ducts or more innovative shielded tubes (see Fig. 15). These latter ones, initially conceived for shielding magnetic fields at extremely low frequencies (i.e., around industrial frequencies), also provide reasonable shielding effectiveness in the RF range.

To the best of the authors' knowledge, other shielding techniques are generally employed at industrial frequencies to reduce magnetic field intensity for environmental purposes to comply

(a) (b)

Fig. 14. (a) Shielding material MRI provided by G-Iron and (b) example of the material installation in a technical room.

Fig. 15. Example of shielded tube for buried cables provided by G-Iron.

with national laws on EM pollution. For instance, techniques based on the principle of deleting sources consist of laying passive loops made of short-circuited cables and ensuring high coupling between source and shield by using magnetic cores. These techniques are particularly effective to shield joint holes of HV cables that are encountered in long HV connections when the grid station is far from the PV field.

Regarding the use of filters, their effectiveness has been tested in the previous paper [9]. Today, various compact EMI filters available on the market can be installed on the PV inverters' dc or ac side. They help control conducted emissions and significantly reduce the potential for HF radiation. When installed on the panel side, they also protect solar panels from stray and leakage currents, which can cause premature aging of the PV modules. These filters are usually designed for low power loss to avoid substantially reducing the overall PV system efficiency.

## VI. Conclusion

Performing in situ EMC tests to characterize conducted and radiated disturbances on modern utility-scale PV plants is not straightforward for a number of technical reasons and external constraints. The technology in this field is constantly improving; unfortunately, most codes and design standards do not adequately catch the upgrade and renovation process in PV fields and their peculiarities. Often, performing such measurements seems more like a work of art than of science. This article revises and updates the EMC challenges commonly encountered in utility-scale PV systems in light of modern trends, compared to what was published in the previous paper [9]. This article examines the issues related to the conductive and radiated RF disturbances in the range from 150 kHz to 1 GHz of multi-MWp PV plants as designed nowadays, with high-power bifacial modules, single-axis trackers, and decentralized high-density inverters. This article presents the results of a measurement campaign of conducted and radiated emission on an actual multi-MWp PV plant, where ambient noise and EM disturbance have been characterized. Analysis and discussion of the results provided a way to devise viable solutions to the EMC challenges and envisage guidelines to pursue *EMC functional safety by design*.

## References


[1] D. Poponi, R. Basosi, and L. Kurdgelashvili, "Subsidisation cost analysis of renewable energy deployment: A case study on the Italian feed-in tariff programme for photovoltaics," *Energy Policy*, vol. 154, 2021, Art. no. 112297.

[2] G. Di Lorenzo, R. Araneo, M. Mitolo, A. Niccolai, and F. Grimaccia, "Review of O&M practices in PV plants: Failures, solutions, remote control, and monitoring tools," *IEEE J. Photovolt.*, vol. 10, no. 4, pp. 914–926, Jul. 2020.

[3] R. Araneo and M. Mitolo, "Insulation resistance and failures of a high-power grid-connected photovoltaic installation: A case study," *IEEE Ind. Appl. Mag.*, vol. 27, no. 3, pp. 16–22, May/Jun. 2021.

[4] M. Di Piazza, C. Serporta, G. Tine, and G. Vitale, "Electromagnetic compatibility characterisation of the DC side in a low power photovoltaic plant," in *Proc. IEEE Int. Conf. Ind. Technol.*, 2004, pp. 672–677.

[5] *IEEE Standard for Interconnection and Interoperability of Distributed Energy Resources With Associated Electric Power Systems Interfaces*, IEEE Standard 1547-2018, 2018.

[6] R. Tonkoski, D. Turcotte, and T. H. M. EL-Fouly, "Impact of high PV penetration on voltage profiles in residential neighborhoods," *IEEE Trans. Sustain. Energy*, vol. 3, no. 3, pp. 518–527, Jul. 2012.

[7] W. Zhang, Y. Wang, P. Xu, D. Li, and B. Liu, "A potential induced degradation suppression method for photovoltaic systems," *Energy Rep.*, vol. 10, pp. 3955–3969, 2023.

[8] V. Rallabandi, O. M. Akeyo, N. Jewell, and D. M. Ionel, "Incorporating battery energy storage systems into multi-MW grid connected PV systems," *IEEE Trans. Ind. Appl.*, vol. 55, no. 1, pp. 638–647, Jan./Feb. 2019.

[9] R. Araneo, S. Lammens, M. Grossi, and S. Bertone, "EMC issues in high-power grid-connected photovoltaic plants," *IEEE Trans. Electromagn. Compat.*, vol. 51, no. 3, pp. 639–648, Aug. 2009.

[10] *Industrial, Scientific and Medical Equipment—Radio-frequency Disturbance Characteristics—Limits and Methods of Measurement*, Int. Special Committee on Radio Interference, Standard CISPR 11, 2015.

[11] *Adjustable Speed Electrical Power Drive Systems—Part 3: EMC Requirements and Specific Test Methods for PDS and Machine Tools*, International Electrotechnical Commission, Geneva, Switzerland, Standard IEC 61800-3, 2022.

[12] *Uninterruptible Power Systems (UPS)—Part 2: Electromagnetic Compatibility (EMC) Requirements*, International Electrotechnical Commission, Geneva, Switzerland, Standard IEC 62040-2, 2016.

[13] *Arc Welding Equipment—Part 10: Electromagnetic Compatibility (EMC) Requirements*, International Electrotechnical Commission, Geneva, Switzerland, Standard IEC 60974-10, 2020.

[14] *Electric Vehicle Conductive Charging System—Part 21-1: Electric Vehicle On-Board Charger EMC Requirements for Conductive Connection to AC/DC Supply*, International Electrotechnical Commission, Geneva, Switzerland, Standard IEC 61851-21-1, 2017.

[15] *Electric Vehicle Conductive Charging System—Part 21-2: Electric Vehicle Requirements for Conductive Connection to an AC/DC Supply—EMC Requirements for Off Board Electric Vehicle Charging Systems*, International Electrotechnical Commission, Geneva, Switzerland, Standard IEC 61851-21-2, 2018.

[16] Y. Karneyeva and R. Wstenhagen, "Solar feed-in tariffs in a post-grid parity world: The role of risk, investor diversity and business models," *Energy Policy*, vol. 106, pp. 445–456, 2017.

[17] J. Andersson, H. Olsson, and A. Theocharis, "Analysis of electromagnetic compatibility in photovoltaic installations validated by site measurements," in *Proc. IEEE Madrid PowerTech*, 2021, pp. 1–6.
[18] Z. Kubík and J. Skála, "Electromagnetic interference from DC/DC converter of photovoltaic system," in *Proc. Int. Conf. Appl. Electron.*, 2019, pp. 1–4.
[19] G. Singh, E. Auel, J. Owens, T. Cooke, M. Stephens, and W. Howe, "Detection of high frequency conducted emission using radiated fields," in *Proc. IEEE PES Innov. Smart Grid Technol. Europe*, 2020, pp. 334–338.
[20] R. Smolenski, P. Lezynski, J. Bojarski, W. Drozdz, and L. C. Long, "Electromagnetic compatibility assessment in multiconverter power systems—conducted interference issues," *Measurement*, vol. 165, 2020, Art. no. 108119.
[21] S. Linder and K. Wiklundh, "In-situ measurements of conducted and radiated emissions from photovoltaic installations," in *Proc. Int. Symp. Electromagn. Compat.*, 2022, pp. 231–236.
[22] U. A. Yusufoglu, T. M. Pletzer, L. J. Koduvelikulathu, C. Comparotto, R. Kopecek, and H. Kurz, "Analysis of the annual performance of bifacial modules and optimization methods," *IEEE J. Photovolt.*, vol. 5, no. 1, pp. 320–328, Jan. 2015.
[23] Y. Li, F. Ye, Y. Liu, N. Yuan, and J. Ding, "Research on the industrial mass production route of N-type passivated contact silicon solar cells with over 23% efficiency," *IEEE J. Photovolt.*, vol. 12, no. 1, pp. 191–197, Jan. 2022.
[24] C. Messmer, A. Fell, F. Feldmann, N. Wöhrle, J. Schön, and M. Hermle, "Efficiency roadmap for evolutionary upgrades of PERC solar cells by TOPCon: Impact of parasitic absorption," *IEEE J. Photovolt.*, vol. 10, no. 2, pp. 335–342, Mar. 2020.
[25] S. Venkateshwarlu, V. S. Pranav, C. S. Anirudh, and K. S. Reddy, "A comparative evaluation of various solar trackers to harness maximum energy—A brief review," in *Proc. Int. Conf. Smart Sustain. Technol. Energy Power Sectors*, 2022, pp. 52–56.
[26] A. Bahrami, C. O. Okoye, and U. Atikol, "Technical and economic assessment of fixed, single and dual-axis tracking PV panels in low latitude countries," *Renew. Energy*, vol. 113, pp. 563–579, 2017.
[27] S. A. Pelaez, C. Deline, P. Greenberg, J. S. Stein, and R. K. Kostuk, "Model and validation of single-axis tracking with bifacial PV," *IEEE J. Photovolt.*, vol. 9, no. 3, pp. 715–721, May 2019.
[28] A. Hafez, A. Yousef, and N. Harag, "Solar tracking systems: Technologies and trackers drive types—A review," *Renew. Sustain. Energy Rev.*, vol. 91, pp. 754–782, 2018.
[29] J. Myrzik and M. Calais, "String and module integrated inverters for single-phase grid connected photovoltaic systems—A review," in *Proc. IEEE Bologna Power Tech Conf. Proc.*, 2003, pp. 1–8.
[30] S.P.A. Terna, "Hypergrid project and development requirements." 2022. Accessed: Jan. 2, 2024. [Online]. Available: https://download.terna.it/terna/2023_Hypergrid_project_and_development_requirements_8db79602cedc732.pdf
[31] R. Araneo and M. Mitolo, *Electrical Safety Engineering of Renewable Energy Systems*. New York, NY, USA: Wiley-IEEE Press, 2022.
[32] S. Yu, J. Wang, X. Zhang, and F. Li, "Complete parasitic capacitance model of photovoltaic panel considering the rain water," *Chin. J. Elect. Eng.*, vol. 3, no. 3, pp. 77–84, 2017.
[33] W. Chen, X. Yang, W. Zhang, and X. Song, "Leakage current calculation for PV inverter system based on a parasitic capacitor model," *IEEE Trans. Power Electron.*, vol. 31, no. 12, pp. 8205–8217, Dec. 2016.
[34] *IEEE Guide for Solar Power Plant Grounding for Personnel Protection*, IEEE Std 2778-2020, 2020.
[35] H. Zhang, S. Wang, and J. Puukko, "Common mode EMI noise modeling and prediction for a three-phase, three-level, grid tied photovoltaic inverter," in *Proc. Asia-Pacific Int. Symp. Electromagn. Compat.*, 2016, pp. 1188–1194.
[36] J. Wang, X. Liu, Y. Xun, and S. Yu, "Common mode noise reduction of three-level active neutral point clamped inverters with uncertain parasitic capacitance of photovoltaic panels," *IEEE Trans. Power Electron.*, vol. 35, no. 7, pp. 6974–6988, Jul. 2020.
[37] *IEEE Guide for Bonding Shields and Sheaths of Single-Conductor Power Cables Rated 5 kV Through 500 kV*, IEEE Standard 575-2014, 2014.
[38] *Photovoltaic Power Generating Systems—EMC Requirements and Test Methods for Power Conversion Equipment*, International Electrotechnical Commission, Geneva, Switzerland, Standard IEC 62920, 2017.
[39] *Electromagnetic Compatibility (EMC)—Part 6-4: Generic Standards—Emission Standard for Industrial Environments*, International Electrotechnical Commission, Geneva, Switzerland, Standard IEC 61000-6-4, 2017.
[40] *Specification for Radio Disturbance and Immunity Measuring Apparatus and Methods—Part 2-3: Methods of Measurement of Disturbances and Immunity—Radiated Disturbance Measurements*, Int. Special Committee on Radio Interference, Standard CISPR 16-2-3, 2016.
[41] M. Mitolo, G. D. Lorenzo, E. Stracqualursi, and R. Araneo, "Equipotential bonding of photovoltaic systems," in *Proc. IEEE 24th Int. Conf. Environ. Elect. Eng.*, 2024, pp. 1–5.
[42] G. Parise, L. Martirano, L. Parise, S. Celozzi, and R. Araneo, "Simplified conservative testing method of touch and step voltages by multiple auxiliary electrodes at reduced distance," *IEEE Trans. Ind. Appl.*, vol. 51, no. 6, pp. 4987–4993, Nov./Dec. 2015.
[43] R. Araneo, M. Maccioni, S. Lauria, and S. Celozzi, "Analysis of the lightning transient response of the earthing system of large-scale ground-mounted PV plants," in *Proc. IEEE Manchester PowerTech*, Jun. 2017, pp. 1–6.
[44] R. Araneo and S. Celozzi, "Transient behavior of wind towers grounding systems under lightning strikes," *Int. J. Energy Environ. Eng.*, vol. 7, no. 2, pp. 235–247, 2016.
[45] SINT Srl, XGSLAB. Accessed: Jan. 2, 2024. [Online]. Available: https://www.xgslab.com/xgslab/general
[46] E. Stracqualursi and R. Araneo, GEA-Simulator. Accessed: Jan. 2, 2024. [Online]. Available: https://sites.google.com/view/geasimulator
[47] S. Celozzi, R. Araneo, P. Burghignoli, and G. Lovat, *Electromagnetic Shielding—Theory and Applications*. Hoboken, NJ, USA: Wiley-IEEE, 2022.

Open Access funding provided by 'Università degli Studi di Roma "La Sapienza" 2' within the CRUI CARE Agreement